Ultra-Deep Azimuth Resistivity sensibilities to a laterally discontinuous reservoir-bed.

Carvalho P. R.* (ICIBE/UFRA), Régis C. R. T. (CPGf/UFPA, INCT/GP) and Silva V. S. (Castanhal/UFPA)

Abstract

Ultra-deep Azimuth Resistivity (UDAR) induction tools have been devised to investigate resistivity structures at some distance away from the borehole, in contrast to the now traditional Triaxial-wireline tools. Here we show a comparative analysis of the sensitivity of these two different profiling sondes with respect to a resistive reservoir bed located a few meters away from the borehole within a more conductive host-formation. To assess the responses of both tools we have numerically generated synthetic data using a tree-dimensional (3D) vector finite element code. The results show that the coaxial and coplanar logs of the Triaxial-wireline have a faint sensitivity to the resistive-bed due to its relatively smaller transmitter-receiver offset and higher frequency, whereas both coil configurations (coaxial and coplanar) of the UDAR-LWD have a visibly better sensitivity than the Triaxial, as is to be expected, because its larger offset and lower operating frequency. Furthermore, unlike the Triaxial-wireline logs, the UDAR-coplanar logs have more sensibility to the resistive-bed than the UDAR-coaxial logs to the three target distances modeled.

Introduction

From the beginning of this century, the need for more information from interbedded sand-shale turbidite sequences prompted the development of the triaxial or multicomponent wireline induction tool, with nine coupling components, that have been successfully used to determine formation anisotropy and bedding dip angle (Kriegshäuser et al., 2000).

Currently, besides being the main location tool of finely laminated reservoirs, triaxial sources and sensors are also applied in many situations of asymmetric geometry, such as locating dissolution cavities (vugs) and fractured zones in the vicinity of the wells, monitoring invasion fronts in horizontal wells, among others (Omeragic et al., 2015).

The introduction of the Ultra Deep Azimuth Resistivity (UDAR) induction tools towards the beginning of the last decade represents a new generation of Logging While Drilling (LWD) geosteering tools providing real time mapping of sedimentary formations, bed-boundaries detection, anisotropy determination, and azimuth resistivity measurements for accurate well placement and formation evaluation, detection of metal cased holes in mature oilfields (Clegg, et al., 2021), and so on.

UDAR tools all use multi-spacing, multi-component and multi-frequency induction measurements to implement the look-around the borehole and look-ahead the drill-bit techniques used in geosteering when the targets are relatively far away.

Instead of reactively geosteering based on to the formation resistivity properties at or behind the drill-bit furnished by conventional LWD tools, these new UDAR-LWD technologies allow proactively navigating based on the formation resistivities several meters around and/or ahead of the bit so that formation boundaries and secondary targets may be now mapped, allowing for improved planning for future wells (Constable et al., 2016).

In addition to this, UDAR technology opened the possibility to integrate with surface seismic data to predict formation change ahead of the bit in real time to make more informed decisions (Mele, et al., 2022).

The simplest multicomponent induction tool (Triaxial wireline and UDAR-LWD) representation consists of three mutually orthogonal coil transmitters and receivers. Figure 1 illustrates two of the nine possible transmitter-receiver combinations within a borehole with diameter $\boldsymbol{D}$: the coaxial configuration, where the dipole moment of the source and the receiver are aligned with the borehole axis, and a coplanar configuration with the dipole moment of the source normal to the axis in the (x, z) plane. In the interest of saving space, these two configurations are the only ones that will be studied here.

The dip angle θ in Figure 1 may be determined by the orientation of the borehole (azimuth and deviation) and the orientation of the formation (dip and strike). This angle can be caused by deviated wells in flat formations, by vertical wells in dipping beds, or by any combination thereof.

Complex apparent conductivities may be calculated from the coaxial σ_a^{cx} and coplanar σ_a^{cp} coil configurations, assuming the sources as vertical (VMD) and horizontal (HMD) point magnetic dipoles, respectively, within an infinite homogeneous isotropic medium (Zhang et al., 2012):

$$\sigma_a^{cx} = \sigma_R^{cx} + i\sigma_X^{cx} = i\frac{4\pi L}{\omega\mu} H_{cx}\,, \qquad (1)$$

$$\sigma_a^{cp} = \sigma_R^{cp} + i\sigma_X^{cp} = i\frac{8\pi L}{\omega\mu} H_{cp}\,, \qquad (2)$$

where $i = \sqrt{-1}$, $\omega = 2\pi f$ is the angular frequency, f is the linear frequency, μ is the magnetic permeability, L is the coil spacing (offset), H_{cx} and H_{cp} are the coaxial and coplanar magnetic field components normal to the planes of the receiver coils, respectively.

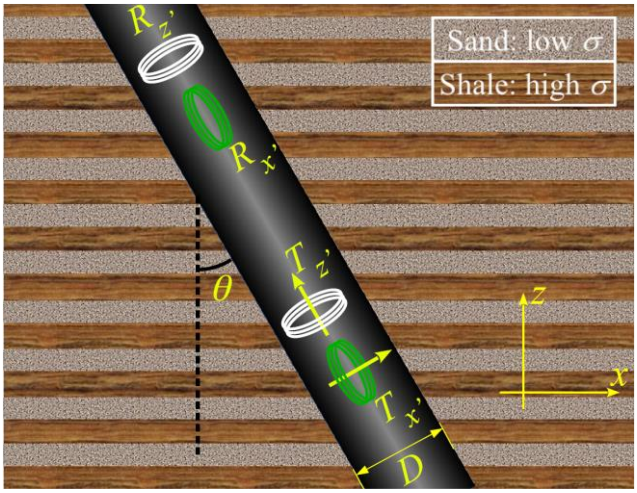

Figure 01 – Illustration of the transmitters and receivers of the coaxial (white) and coplanar (green) configurations within a laminated formation traversed by a borehole.

The real parts σ_R^{cx} and σ_R^{cp} are named quadrature or resistive components and the imaginary parts σ_X^{cx} and σ_X^{cp} are the inphase or reactive components.

The coaxial and coplanar mutual coupling signals are part of the imaginary parts of the conductivities and are several orders of magnitude greater than the formation signals. Actual field tools usually contain additional "bucking" coils to cancel these large mutual coupling signals. However, since it is straightforward to calculate analytically and remove them computationally (Anderson et al. 2002) we do not model bucking coils. Thus, the imaginary parts of the apparent conductivity without direct coupling are denoted by σ_{XF}^{cx} and σ_{XF}^{cp}.

The coaxial (σ_c^{cx}) and coplanar (σ_c^{cp}) apparent conductivities corrected for the skin effect (signal level attenuation and phase shift) are obtained by

$$\sigma_c^{cx} = \sigma_R^{cx} \,/\, B^{cx}, \qquad (3)$$

$$\sigma_c^{cp} = \sigma_R^{cp} \,/\, B^{cp}, \qquad (4)$$

where

$$B^{cx} = 1 - \frac{2}{3}\left(\frac{L}{\delta}\right) + \frac{2}{15}\left(\frac{L}{\delta}\right)^3 - \frac{1}{18}\left(\frac{L}{\delta}\right)^4 + \frac{1}{105}\left(\frac{L}{\delta}\right)^5 \qquad (5)$$

$$B^{cp} = 1 - \frac{4}{3}\left(\frac{L}{\delta}\right) + \frac{8}{15}\left(\frac{L}{\delta}\right)^3 - \frac{5}{18}\left(\frac{L}{\delta}\right)^4 + \frac{2}{35}\left(\frac{L}{\delta}\right)^5 - \frac{8}{2835}\left(\frac{L}{\delta}\right)^7 + \frac{1}{4000}\left(\frac{L}{\delta}\right)^8 - \frac{1}{12474}\left(\frac{L}{\delta}\right)^9. \qquad (6)$$

The terms of the coaxial (B^{cx}) and coplanar (B^{cp}) boosters are obtained from the imaginary parts of the apparent conductivities σ_{XF}^{cx} and σ_{XF}^{cp}, respectively, which are exactly equal to those in the real parts σ_R^{cx} and σ_R^{cp}. We show the coplanar booster (Eq. 6) with almost twice as many terms as the coaxial (Eq. 5) because of its well-known (Anderson et al., 2002) strongest skin effect.

A first order skin effect correction to the coaxial (Moran & Kunz, 1962) and coplanar (Carvalho & Verma, 1999) signals, i.e., up to the second term of the infinite series of the boosters (Eq. 5 and 6), is sufficient to the conventional induction logs (Triaxial wireline) which the coil spacings $L \approx 1.0$ m are relatively low compared to those of the UDAR-LWD which are tens of meters.

According Puzyrev et al. (2018) typical transmitter-receiver offsets for the latest generation of UDAR technology ranges from 5 m to 35 m and matches the scales of many reservoir environments and overlaps with the surface-seismic resolution.

The UDAR evolution from look-around to look-ahead capability is dependent on the coil spacings, frequencies, resistivity around the tool, bed thicknesses and resistivity contrast of the target.

The Depth of Investigations (DOI) of the induction tools depends on the spatial distribution of the electromagnetic fields in the conductive medium, which is dominated by two controlling factors, namely 1) the exponential attenuation as a function of skin depth and 2) the geometric spreading inversely proportional to the distance cubed. The electromagnetic fields fade away rapidly due to skin effect, and consequently, so is the associated sensitivity function. The smaller field or poorer sensitivity far away from the tool also dictates that the resolution farther away from the tool is much worse than the resolution near the tool (Zhu, et al., 2021).

Thus, the DOI defines how much is “Look-around” or how much is “Look-ahead” and, because of that, the providers get accused of "black box" solutions, which fail to communicate the understanding of the underlying tool responses (Rabinovich and Martakov, 2012). A rule of thumb is that the DOI is equal to the maximum coil spacing in high resistivity environments and is halved in conductive formations (Puzyrev et al., 2018).

Our goal in this work is to investigate the sensibilities of the triaxial-wireline and UDAR-LWD (coaxial and coplanar

configurations) tools to a laterally discontinuous reservoir-bed due to a normal geological fault, for example, a few meters away from a borehole filled with a water-based mud (Fig. 2).

Method

The layered 1D problem is formulated using the mathematical tools described by Kaufman and Ytskovich (2017), generalized to multi-layered TIV media. The solutions are written as integrals of the Hankel transform, which are evaluated numerically using the Quadrature With Extrapolation (QWE) method as presented by Key (2012).

The 3D problem is solved with an implementation of the Vector Finite Element method, using a secondary magnetic field formulation, and following the steps presented by Jin (2015). The dipole sources are in an infinite homogeneous isotropic space with the same conductivity as the drilling mud that simulates the environment inside the borehole. This choice for the primary medium means that the secondary media occupy all the space outside the borehole, so that the primary electric field from the sources needs to be calculated in a great number of points in the mesh. However, it presents two important advantages: it will easily allow the simulation of different geometries for the borehole in future work, and it results in the primary electric field being calculated using an extremely simple analytical formula with minimum computational effort.

The problem is formulated to solve directly for the secondary magnetic field, which obviates the need to calculate numerical derivatives.

The system of linear equations generated by the Vector Finite Element method needs to be solved twice (once for each dipole) for every tool position in the profile, in all cases with the same complex sparse coefficient matrix. We chose to use the direct parallel solver PARDISO (Schenk et al., 2001), because a direct approach allows the factoring of the coefficient matrix only once, solving the multiple systems every time with only a phase of forward and backward substitutions. This means that the problem can be solved in shorter times than with an iterative solution. The software package PARDISO is implemented with an efficient memory management that stores only the non-zero elements of the matrix in every step of the factorization, which allows working with systems that would be simply impossible to fit in memory if the full matrix needed to be stored.

The 3D tetrahedral meshes were generated using the Tetgen software (Si, 2015). The mesh outer boundaries are built following the cylindrical geometry of the well and invasion zones. The radius from the well axis to the outer boundary of the mesh must be big enough to allow the application of homogeneous boundary conditions in the secondary magnetic field. The optimum radius depends on the frequency and range of resistivities in the model.

Results

This work compares the responses of the triaxial-wireline and UDAR-LWD (coaxial and coplanar configurations) tools, generated by 3D Vector Finite Element program, for a reservoir-bed model (Fig. 2) of thickness H = 8 m and D = 5, 10 and 20 meters away from a borehole filled with a mud resistivity of 5 ohm-m. The frequencies and transmitter-receiver offsets are: 1) Triaxial-wireline: 20 kHz and 1.0 m and 2) UDAR-LWD: 5 kHz and 20 m.

Figure 3 shows a validation test with a comparison of the 3D and 1D UDAR vertical logs for a 100 ohm-m reservoir-bed within a 5 ohm-m host formation. In this case, to simulate the measurements in the 3D code, the borehole diameter is assumed exceedingly small (6 cm) and the mud resistivity (5 ohm-m) equal to the host rock. In these conditions, it is expected that the borehole effects on the 3D responses are minimal and the 1D and 3D logs are very similar.

The results show a good agreement between the 1D and 3D solutions, except for a slight departure from the coplanar curves (right) due to numerical noise, when the analytical response is a straight vertical line, i.e., when the bed is between the transmitter-receiver coils.

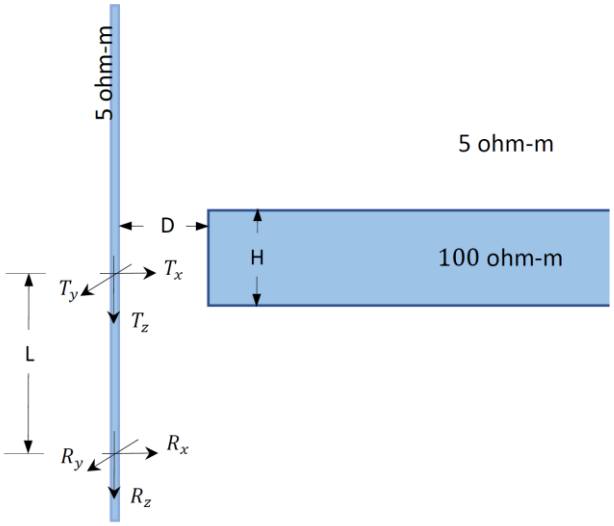

Figure 02 – Illustration of a induction multicomponent tool (triaxial-wireline or UDAR-LWD) within a vertical borehole in front of a laterally discontinuous reservoir-bed.

The coplanar logs are more sensitive to the bed-boundaries than the coaxial logs because of the so-called “polarization” horns. These coplanar horns have been shown by Régis et al. (2020) to be associated with the discontinuous current density field parallel to the interfaces between layers, rather than with surface charge build-up from the continuous current across the interface, as was universally accepted since the early 1990s. They are unavoidable features of the coplanar logs and are slightly smoothed by the influence of the well, a difference

hard to notice for this thin well, but more pronounced in regular wider wells.

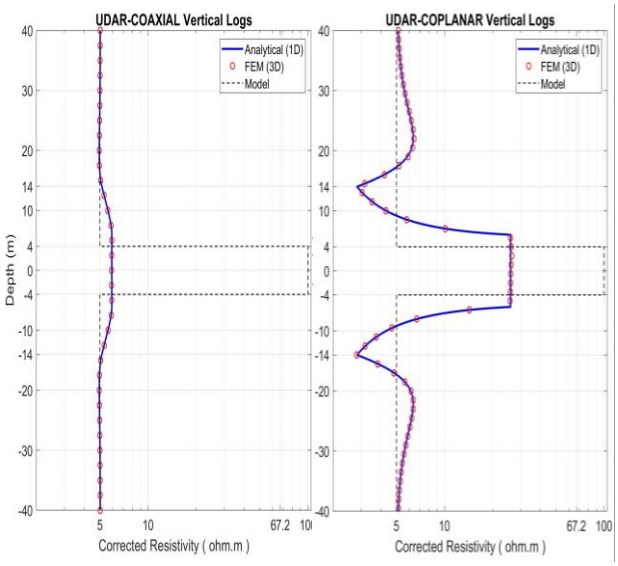

Figure 03 – Validation test. Coaxial (left) and coplanar (right) vertical responses of the UDAR-LWD generated by a 1D analytical code (solid blue line) and the 3D vector finite element code (circle red line).

These benchmarking results indicate a good validation between 1D and 3D responses, i.e., less than 1% within the bed-reservoir, that gives us confidence in the accuracy for more complicated geometries.

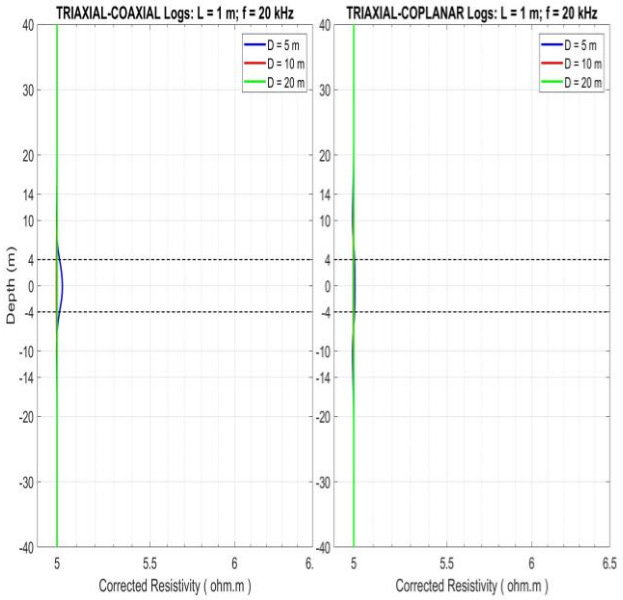

Figure 04 – Triaxial-wireline coaxial (left) and coplanar (right) vertical logs in front of a laterally discontinuous resistive-bed (100 ohm-m) within a conductive-host (5 ohm-m) and 5, 10 and 20 meters away from the borehole.

Figure 4 shows the triaxial-wireline coaxial (left) and coplanar (right) responses have a faint sensibility to a laterally discontinuous thick (8 m) resistive-bed (100 ohm-m) within a conductive formation-host (5 ohm-m), placed at 5 m (blue lines) away from the borehole (20 cm diameter and 5 ohm-m mud resistivity) while for the distances of 10 m and 20 m, all responses are practically blind to the presence of the target. This is due to its relatively smaller triaxial-wireline transmitter-receiver offset (1 m) and higher frequency (20 kHz).

Figure 5 shows the UDAR-LWD coaxial (left) and coplanar (right) responses have a best sensibility than the triaxial-wireline to the same resistive-model of the Fig. 4. This is due to its relatively higher transmitter-receiver offset (20 m) and smaller frequency (5 kHz). Furthermore, unlike the Triaxial-wireline logs, the UDAR-coplanar logs (right) have more sensibility to the resistive-bed than the UDAR-coaxial logs (left) to the three target distances.

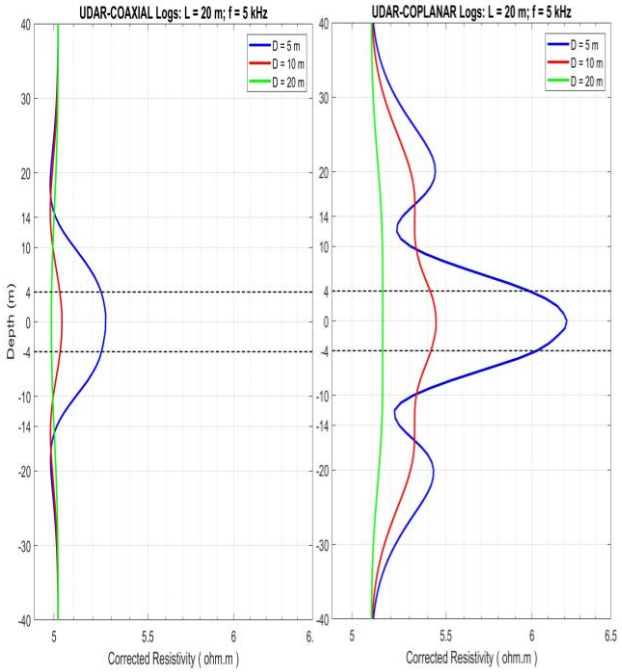

Figure 05 – UDAR-LWD coaxial (left) and coplanar (right) vertical logs in front of a laterally discontinuous resistive-bed (100 ohm-m) within a conductive-host (5 ohm-m) and 5, 10 and 20 meters away from the borehole.

Conclusion

In this paper, we modeled some numerical responses, generated by 3D vector finite element code, to develop a comparative analysis of the triaxial-wireline and the UDAR-LWD logs, in front of a discontinuous reservoir-bed, within a more conductive host-formation, some meters away from the borehole filled by a water-based mud.

The results show that the coaxial and coplanar logs of the triaxial-wireline have a faint sensibility to the resistive-bed due to its relatively smaller transmitter-receiver offset and higher frequency. Meanwhile, both coil configurations, (coaxial and coplanar) of the UDAR-LWD have a visibly better sensitivity than the triaxial, as is to be expected, because its larger offset and lower operating frequency.

Furthermore, unlike the Triaxial-wireline logs, the UDAR-coplanar logs have more sensibility to the resistive-bed than the UDAR-coaxial logs to the three target distances modeled.

Acknowledgments

Paulo Carvalho thanks the Cyberspace Institute (ICIBE) of the Federal Rural University of Amazonia (UFRA) for the research support. Both authors thank Petrobras for the support of this research through project number 2017/00424-6.

References

Anderson, B. I.; Barber, T. & Habashy, T. M. 2002. The interpretation and inversion of fully triaxial induction data; a sensitivity study. In: Annual Logging Symposium, 43rd. Oiso, Japan. Anais SPWLA. Paper O.

Carvalho, de P. R. & Verma, O. P. 1999. Coplanar coils response in a borehole. 6th International Congress of the Brazilian Geophysical Society. Rio de Janeiro, RJ, Brazil. http://earthdoc.eage.org/publication/publicationdetails/?publication=47940

Clegg, N.; Duriez, A.; Kiselev, V.; Sinha, S.; Parker, T.; Jakobsen, F.; Jakobsen E.; Marchant, D. & Schwarzbach, C. 2021. Detection of offset wells ahead of and around an LWD ultra-deep electromagnetic tool. In: Annual Logging Symposium, 62nd. Virtual event. Anais SPWLA. Paper Number: 0039. https://doi.org/10.30632/SPWLA-2021-0039

Constable, M. V.; Antonsen, F.; Stalheim, S. O.; Olsen, P. A.; Fjell, Ø. Z.; Dray, N.; Eikenes, S.; Aarflot, H.; Haldorsen, K.; Digranes, G.; Seydoux, J.; Omeragic, D.; Thiel, M.; Davydychev, A.; Denichou, J.; Salim, D.; Frey, M.; Homan, D. & Tan, S. 2016. Looking ahead of the bit while drilling: from vision to reality. In: Annual Logging Symposium, 57th. Reykjavik, Iceland. Anais SPWLA. Paper MMMM.

Jin, J.-M., 2015, The finite element method in electromagnetics, third ed.: Wiley, 800 pp.

Key, K., 2012, Is the fast hankel transform faster than quadrature? GEOPHYSICS, 77, F21–F30, https://doi.org/10.1190/geo2011-0237.1.

Kriegshäuser, B.; Fanini, O.; Forgang, S.; Itskovich, G.; Rabinovich, M.; Tabarovsky, L. & YU, L. 2000. A new multicomponent induction logging tool to resolve anisotropic formations. In: Annual Logging Symposium, 41st. Dallas, Texas, USA. Anais SPWLA. Paper D.

Mele, M.; Chinellato, F.; Leone, M.; Borahi, M., Tosi, G. & Tveit, J. A. 2022. The Impact of Ultradeep Azimuthal Resistivity Technology on ENI Geosteering Workflow Evolution. In: Annual Logging Symposium, 63rd. Stavanger, Norway. Anais SPWLA. Paper Number: 0044. https://doi.org/10.30632/SPWLA-2022-0044

Moran, J. H. & Kunz, K. S. 1962. Basic theory of induction logging and application to study of two coil sondes. Geophysics, 27 (6): 829-858.

Omeragic, D.; Bayraktar, Z.; Thiel, M.; Habashy, T.; Alatrach, S. & Shray, F. 2015. Triaxial induction interpretation in horizontal wells: mapping boundaries, characterizing anisotropy and fractures. In: Annual Logging Symposium, 56th. Long Beach, California, USA. Anais SPWLA. Paper I.

Puzyrev, V.; Torres-Verdín, C. & Calo, V. 2018. Interpretation of deep directional resistivity measurements acquired in high-angle and horizontal wells using 3-D inversion. Geophysical Journal International, v.213(2), pg. 1135-1145. https://doi.org/10.1093/gji/ggy047

Rabinovich, M.; Lofts, J. & Martakov, S. 2012. The vagaries and myths of look-around deep resistivity measurements while drilling. Petrophysics, v.53, no. 2, pg. 86-101.

Régis, C.; Carvalho, P. R. & Silva, S. S. 2020. A new look at the causes of “polarization” horns in electromagnetic well logging. Geophysics, v.85, no 6. https://doi.org/10.1190/geo2020-0163.1

Schenk, O., K. Gärtner, W. Fichtner, and A. Stricker, 2001, Pardiso: a high-performance serial and parallel sparse linear solver in semiconductor device simulation. Future Generation Computer Systems, 18, 69–78, https://doi.org/10.1016/S0167-739X(00)00076-5.

Si, H., 2015, Tetgen, a Delaunay-based quality tetrahedral mesh generator: ACM Trans. Math. Softw., 41, 1–36, https://doi.org/10.1145/2629697.

Zhang, Z.; Boyuan, Y. & Liu, C. 2012. Investigation of Effects of large dielectric constants on triaxial induction logs. Applied Mathematics, v.3, 1811-1817. http://dx.doi.org/10.4236/am.2012.331246